Table of Contents

The dual-functional CB/PEDOT:PSS modified separator is fabricated by facile fabrication. By providing effective polysulfides absorption and better current transportation, this light-weight coating brings a capacity of 956 mAh g^{-1} after 100 cycles at 0.2C and a 522 mAh g^{-1} total cathode mass capacity at 1 C

Graphical Abstract

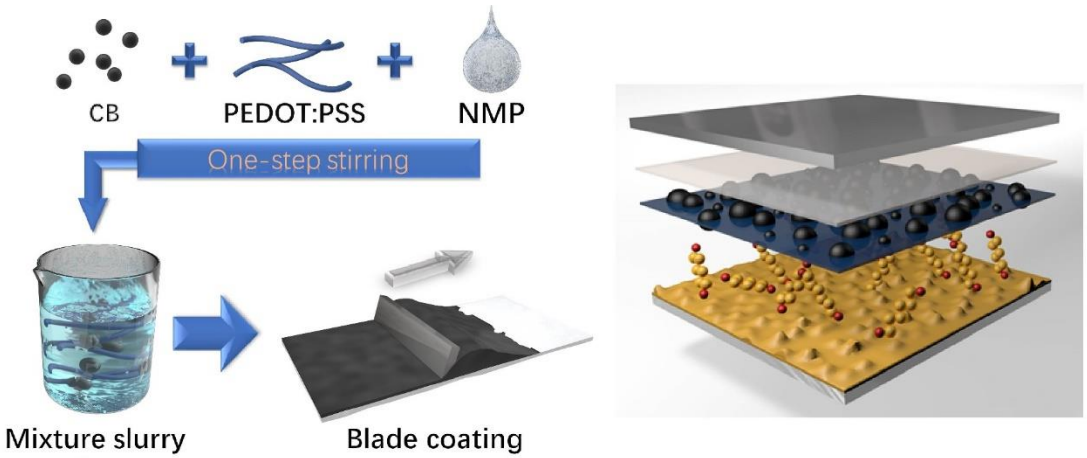

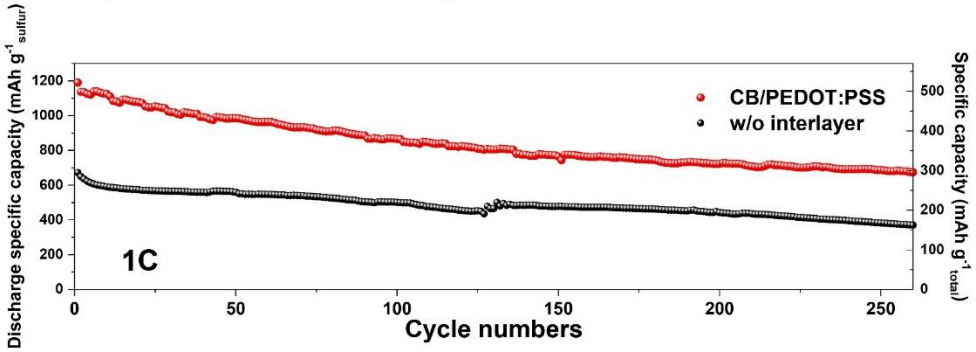

The Facile Fabrication of a Light-weight Dual-functional Modified Separator towards High Performance Li-S Batteries

Ruowei Yi[a,b], Xiangfei Lin[a], Yinchao Zhao[c,d], Chenguang Liu[c,d], Yinqing Li[e], Laurence J. Hardwick[b], *Li Yang[a], *Cezhou Zhao[c], Xianwei Geng[c,d], Qian Zhang[a]

[a] *Ruowei Yi, Xiangfei Lin, Dr. Li Yang, Dr. Qian Zhang*

Department of Chemistry, Xi'an Jiaotong-Liverpool University, Suzhou, Jiangsu 215123, China

[b] *Ruowei Yi, Prof. Laurence J. Hardwick*

Stephenson Institute for Renewable Energy, Department of Chemistry, University of Liverpool, Liverpool L69 7ZD, UK

[c] *Yinchao Zhao, Chenguang Liu, Prof. Cezhou Zhao, Xianwei Geng*

Department of Electrical and Electronic Engineering, Xi'an Jiaotong-Liverpool University, Suzhou 215123, China

[d] *Yinchao Zhao, Chenguang Liu, Xianwei Geng*

Department of Electrical Engineering and Electronics, University of Liverpool, Liverpool L69 3GJ, UK

[e] *Yinqing Li*

Dongguan Hongde Battery Ltd.Co., Dongguan 523649, China

*Corresponding authors

*Corresponding authors

E-mail addresses: li.yang@xjtlu.edu.cn (L. Yang); cezhou.zhao@xjtlu.edu.cn (C. Zhao)

Keywords: Lithium-sulfur battery; interlayer; PEDOT:PSS; polysulfides

Keywords: Li-S battery; Interlayer; poly (3,4-ethylene dioxythiophene) : poly (styrene sulfonate)

Abstract

A light-weight dual-functional modified separator for lithium-sulfur batteries is prepared by a facile physical blend and blade-coating approach. The separator is coated by carbon black/ poly (3,4-ethylene dioxythiophene) : poly (styrene sulfonate) (CB/PEDOT:PSS), remarkably improving the utilization of sulfur by serving as the co-current collector. Moreover, the PEDOT:PSS effectively inhibits the diffusion of polysulfides and promotes the migration of lithium ions through providing chemical absorption and cation transport acceleration. When assembling this modified separator into the coin cell, an initial specific capacity of 1315 mAh g^{-1} at 0.2 C is achieved with a capacity of 956 mAh g^{-1} after 100 cycles, showing a superior improved performance compared to the cell without interlayer. Meanwhile, the cell exhibits a rate capability with a discharge capacity of 699 mAh g^{-1} at a current density of 2 C. Notably, the areal density of CB/PEDOT:PSS coating is as low as 0.604 mg cm^{-2}, bringing a specific electrode capacity of 522 mAh g^{-1} at 1 C.

Introduction

Lithium-sulfur (Li-S) batteries have been broadly investigated over the past decades, as they deliver high specific capacity of 1672 mAh/g and high energy density of 2600Wh/kg that are much higher than those of commercial lithium ion batteries (LIBs) [1]. Besides, the elemental sulfur also surpasses other cathode materials for its low-cost, natural abundance and environmental benignity [2]. However, the commercial applications of Li-S batteries are still hindered by several crucial drawbacks: the poor electrical and ionic conductivities of sulfur and related discharge products seriously retard the redox reaction. In addition, originated from the soluble long-chain polysulfides, the so called “shuttle effect” can contaminate the Li anode and cause active material lost, consequently degrading the capacity performance over long term cycles [3-6].

To overcome these obstacles, tremendous efforts have been made and many strategies focus on combining sulfur with conductive host, including carbon nanotubes [7-9], graphene [10-12], porous carbon [13, 14], 2D layered transition metal carbides and/or nitrides (MXene) [15, 16] and conductive polymers [17-19]. By applying these tactical strategies, the sulfur composites show much improved specific capacity and cycling stability than the pristine sulfur cathode. Meanwhile, some researchers are interested in building a functional interlayer between the cathode and the separator [20]. This kind of battery configuration is usually fabricated in an existence of free-standing layer [21-24], or as a surface coating on the separator [25-28] or the cathode [29, 30]. Functionally, this additional layer benefits the Li-S batteries by providing enhanced

electron conductivity of sulfur cathode, polysulfides adsorption and anode protection [20]. Furthermore, to enhance the long-term performance, researchers tried to apply materials with polarized surface into the interlayer, especially some non-conductive metal oxides, as an effective way to anchor the dissolved active materials over many cycles [30-32]. Some conductive polymers have also been reported as the polysulfides trapping materials, such as polyaniline (PANi) [19, 33-35], poly(3,4-ethylene-dioxythiophene) (PEDOT) [36, 37] and polypyrrole (PPy) [38]. The heteroatoms with lone electron pairs (such as oxygen, nitrogen, and sulfur atoms) in these conductive polymers are able to chemically bind with the lithium atom in lithium sulfides species [17], which endows the polymers with an ability to mitigate the shuttle effect. As remarkable conductors, these polymers with preeminent polysulfide-trapping ability exhibit attractive advantages over other nonconductive adsorbents, as the latter usually result in greater ohmic polarization and prevent the adsorbed polysulfides from receiving the electrons, thus hindering the chemical redox process. Wen's group applied Ppy [29] and Ppy nanotubes film [38] as interlayers between cathode and separator, and successfully improved both initial specific capacity as well as the long-term cycling performance. Besides, the PANi-graphene oxide (GO) interlayer fabricated by Dou's group also showed a remarkable effect on cycling stability and much improved rate performance on sulfur cathode [39]. It is worth noting that Cui's group has investigated different conductive polymers as the coating shell of nano-sized sulfur, and they demonstrated that PEDOT exhibits the best performance over PANi and Ppy on improving long-term cycling stability and high-rate performance [17]. Other

researchers also proved the macromolecular salt of PEDOT or PEDOT:PSS serve well as the polysulfides absorber in the interlayer [40].

Despite all the benefits brought by the interlayers, these novel configurations are usually not suitable for scale-up application, either involving multistep processes or harsh conditions, consuming much time and labor source. These drawbacks will eventually lift the cost of batteries, preventing the ultimate scale-up industrial manufacturing. As a result of tackling to those issues, it was seen the development of carbonaceous interlayers fabricated by facile methods [28, 41, 42]. However, their strategies on polysulfide-trapping are usually limited in physical absorption, which shows a more severe capacity degradation due to the weak van der Waals' force absorption mechanism, especially when tested for a long term [43]. Hence, for the scale-up production of high-performance Li-S batteries, it is crucial to find a facile and scalable approach to fabricate interlayers which combines both physical and chemical absorption abilities.

Herein, we designed a bifunctional carbon black/PEDOT:PSS (CB/PEDOT:PSS) modified separator with a facile approach, which greatly ameliorates the capacity and cycling performance of Li-S batteries and favors the scale-up production. This highly conductive interlayer coating on the separator serves not only as a co-current collector but an efficient polysulfides trapper, delivering an initial specific capacity of 1315 mAh g^{-1} at 0.2 C, 93.1 % higher than the cell without an interlayer. After 100 cycles the cell with the CB/PEDOT:PSS interlayer maintained a capacity of 956 mAh g^{-1}. Also, the rate performance of the cell demonstrated its capability to deliver high capacity at

different rates. Meanwhile, the low areal density of this coating helps the cell maintaining a practical 522 mAh g^{-1} specific electrode capacity. Most importantly, this high-performance interlayer can be fabricated by a one-step facile method of physical blend under ambient condition, along with conventional blade-coating process, being labor-saving and industrial favorable. Therefore, it is expected that this CB/PEDOT:PSS modified separator has great potential for future applications in low-cost and high-performance Li-S batteries.

Experimental section

Fabrication of CB/PEDOT:PSS modified separator

Carbon black (super-P, Timical, Switzerland), poly(vinylidene fluoride) (PVDF, ⩾ 99.5%,) and CB/PEDOT:PSS particles (Agfa, vacuum dried at 60 °C for 12h before used) were well mixed in a weight ratio of 40:4:5 in N-methyl-2-pyrrolidone (NMP, Aladdin). The slurry was magnetically stirred for 24 h in order to disperse PEDOT:PSS well and improve the uniformity of the slurry. The homogeneous slurry was blade-coated on a Celgard 2400 separator via doctor blade coating. The coated separator was desiccated in vacuum at 50 °C overnight. The resulting separator was denoted as CB/PEDOT:PSS separator. The pure carbon black modified separator was prepared following the same procedure and was marked as CB separator. The typical areal densities of the interlayers coating are 1.12 mg cm^{-2} for CB and 0.604 mg cm^{-2} for CB/PEDOT:PSS.

Electrode preparation

The S-C electrode was fabricated by mixing 60 wt% sulfur with 30 wt% conductive CB as a conducting agent and 10 wt% PVDF as a binder in the NMP. The slurry was magnetically stirred for 24 h to achieve greater homogeneity. After stirring, the slurry was coated on a 20 μm thick aluminum foil current collector by a blade-coating machine, followed by a vacuum desiccation at 60 °C for 12 h. The prepared electrodes were cut into discs of diameter 13 mm for coin cell assembling. A typical mass loading of the active materials was ~ 1.6 mg/cm^2.

Materials characterization

The morphology and elemental mapping of the CB and CB/PEDOT:PSS interlayers were observed using a scanning electron microscope (SEM, JEOL JSM-6510) and an energy dispersive X-ray spectrometer (EDS, PENTA FET Precision). The X-ray photoelectron spectroscopy (XPS, ESCALAB 250Xi, Thermo scientific) was conducted using Al Kα X-ray source. The current-voltage curves were collected by the Autolab PGSTAT302N electrochemical workstation using 1 cm × 4 cm rectangular samples.

Electrochemical measurements

The S-C electrode and interlayer were tested in two-electrode 2032 coin-type cells using Li foil as counter electrodes. The cells were assembled in an argon-filled glove box. The electrolyte was 1.0 M lithium bis (trifluoromethanesulfonyl) imide (LiTFSI) in dioxolane (DOL) and dimethoxyethane (DME) (1:1 by volume) with a 1.0 wt% $LiNO_3$ additive. The amount of electrolyte is 50 μL for each cell. The Li-S cell without any interlayer is denoted as w/o interlayer. The CB and CB/PEDOT:PSS modified separators were cut into discs of 18 mm in diameter and placed with the coating facing towards S-C working electrode. Galvanostatic charge/discharge tests were performed in the potential range of 1.5-2.8 V at 25 °C with the Neware CT-4008 battery-testing system.

Results and discussion

Scheme 1 shows the fabrication process of CB/PEDOT:PSS modified separator. The slurry was prepared by one-step method that only involves physical mixing. Therefore, this process has great potential to be integrated into the existing industrial production.

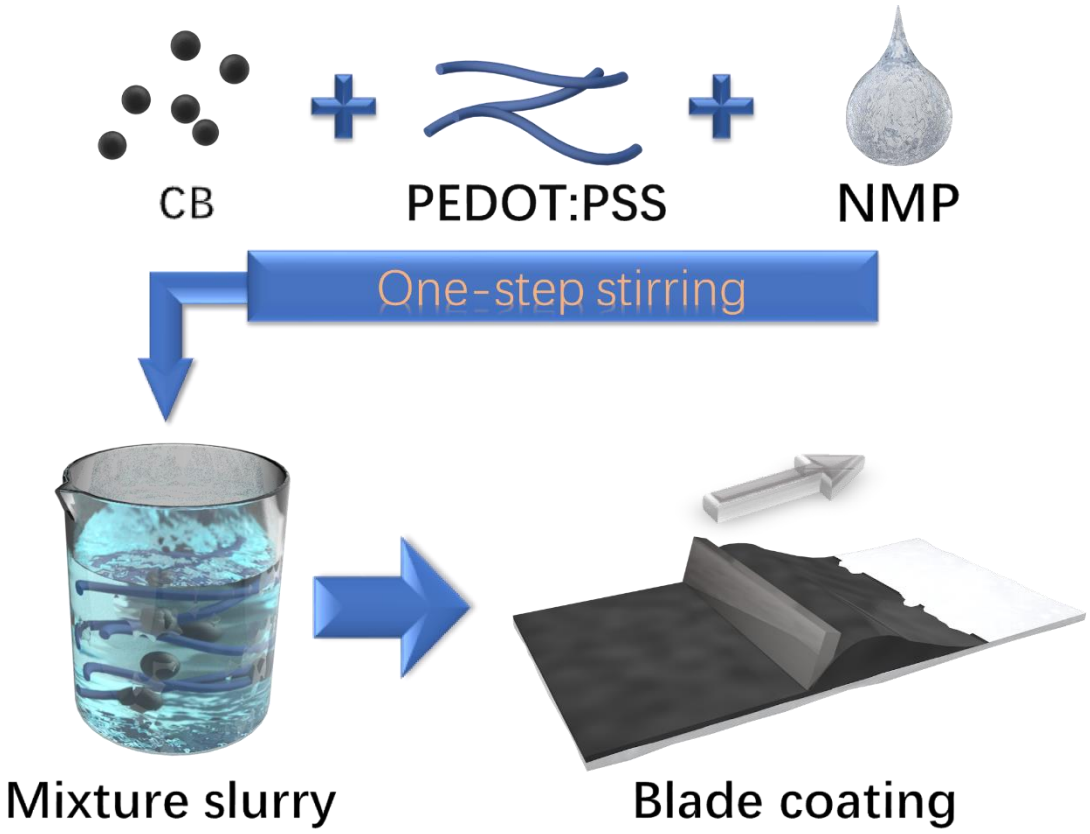

Scheme 1. The preparation of CB/PEDOT:PSS modified separator.

The morphology of the as-prepared CB/PEDOT:PSS interlayer surface was observed by SEM. The cross-section of this modified separator shows this CB/PEDOT:PSS coating has a thickness of around 6.4 μm, as shown in Fig. 1a, taking up only 35.5% of the Celgard separator's thickness (18.0 μm), as denoted in the figure. The specific surface area and pore information on CB/PEDOT:PSS coating were measured by nitrogen adsorption−desorption isotherms (Fig S1). The Brunauer−Emmett−Teller

(BET) specific surface area and pore volume are 52.0 m^2/g and 0.18 mL/g, respectively. The pore size distribution, as shown in the inset of Fig. S1, indicates abundant mesopores centered at 2.5 nm. Such rough and porous surface of this interlayer offers great chance to trap polysulfides and provides unimpeded channels for Li ion between anode and cathode. The PEDOT:PSS not only enhances the physical strength by acting as the additional binder between carbon particles, but also improves the electronic transmission of the CB/PEDOT:PSS composite by providing extra electron pathways between carbon particles. As a result, the CB/PEDOT:PSS interlayer presents better conductivity than CB interlayer (see later discussion).

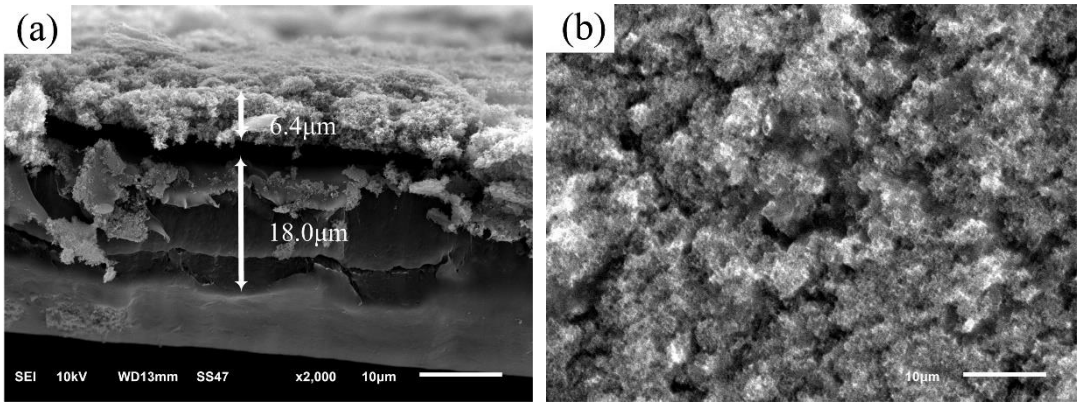

Fig. 1. (a) Side view of the CB/PEDOT:PSS modified separator, the thickness of the separator and coating layer was marked by arrows; (b) SEM image of the CB/PEDOT:PSS interlayer.

The improved conductivity of CB/PEDOT:PSS modified separator is confirmed by the comparison of current-voltage (*I-V*) curves for pristine Celgard, CB and CB/PEDOT:PSS modified separators (Fig. S2). Tested by the linear sweep voltammetry, the CB/PEDOT:PSS modified separator shows the largest slope value, followed by the CB and Celgard separator. Since the slope value is proportional to the electrical conductivity of the separator, our results reveal that the CB/PEDOT:PSS modified

separator has the highest electrical conductivity among the three different separators. The specific resistivity values of three separators were measured by the four probes method as shown in Table S1. This striking conductivity difference in the CB/PEDOT:PSS modified separator provides “high-way” for the electron transportation. The conductivity refinement is due to that the “point-to-point” contact between two carbon particles is replaced with the large area contact brought by the PEDOT:PSS. Therefore, the CB/PEDOT:PSS modified separator can better facilitate the redox reaction of the active material than CB and pristine separators.

Configuration of the Li-S cell with the CB/PEDOT:PSS interlayer is shown in Scheme S1. The CB/PEDOT:PSS was coated on one side of the Celgard separator (towards the cathode side). This conductive CB/PEDOT:PSS interlayer acts as a co-current collector to improve the specific capacity of the cell. Meanwhile, the carbon black and PEDOT:PSS components in the interlayer provide physical and chemical anchor for polysulfides, respectively, which greatly suppresses the shuttle effect and enhances the utilization of sulfur species.

The typical galvanostatic charge/discharge behaviors at the 2^{nd} cycle of different cells at 0.2 C are presented in Fig. 2. All the cells show one charge plateau at ~ 2.3 V and two discharge plateaus ~ 2.3 V and ~ 2.0 V, which represent typical redox reactions of sulfides oxidation and two-step sulfur reduction [14]. The cell without interlayer shows a specific capacity of 679 mAh g^{-1}, only 40.6 % of the theoretical capacity. For the cells with CB or CB/PEDOT:PSS interlayers, much higher capacities (947 mAh g^{-1} and 1370 mAh g^{-1}) are achieved, which are 56.5 % and 81.9 % of the theoretical capacity,

respectively. The insert in Fig. 2 shows the enlarged part where two discharge plateaus meet. It is clear that for the cell without interlayer a “potential dip” is observed at the beginning of the low-voltage plateau. This can be attributed to the accumulation of insulate high-order polysulfides during the first reduction step, which increases the resistance of cathode and hinders further reduction [25]. Also, the concentration of the dissolved polysulfides in electrolyte reaches its maximum at this point, resulting in high viscosity of the electrolyte. Therefore, extra overpotential is needed to trigger the consequent reduction into Li_2S_2/Li_2S. When the potential drops to the value where high-order polysulfides begin to be reduced to Li_2S_2/Li_2S, the viscosity of electrolyte decreases and so does the polarization of the cell, therefore a “potential dip” occurs at the beginning of the second discharge plateau [38]. For the cell with CB interlayer, the dip is not obvious, and for the CB/PEDOT:PSS interlayer one this barrier almost disappears. This variation in the voltage barrier indicates the interlayers remit the influence of the polysulfides accumulation by improving conductivity and absorbing the dissolved polysulfides. In Fig. 2b-d, the charge/discharge curves of different cells at various current rates also confirm that the CB/PEDOT:PSS cell has superior performance in terms of sulfur utilization even at 2 C rate. By applying the PEDOT:PSS as a chemical anchor, the CB/PEDOT:PSS interlayer is evidenced to be more effectively in polysulfide-trapping than the pure CB interlayer.

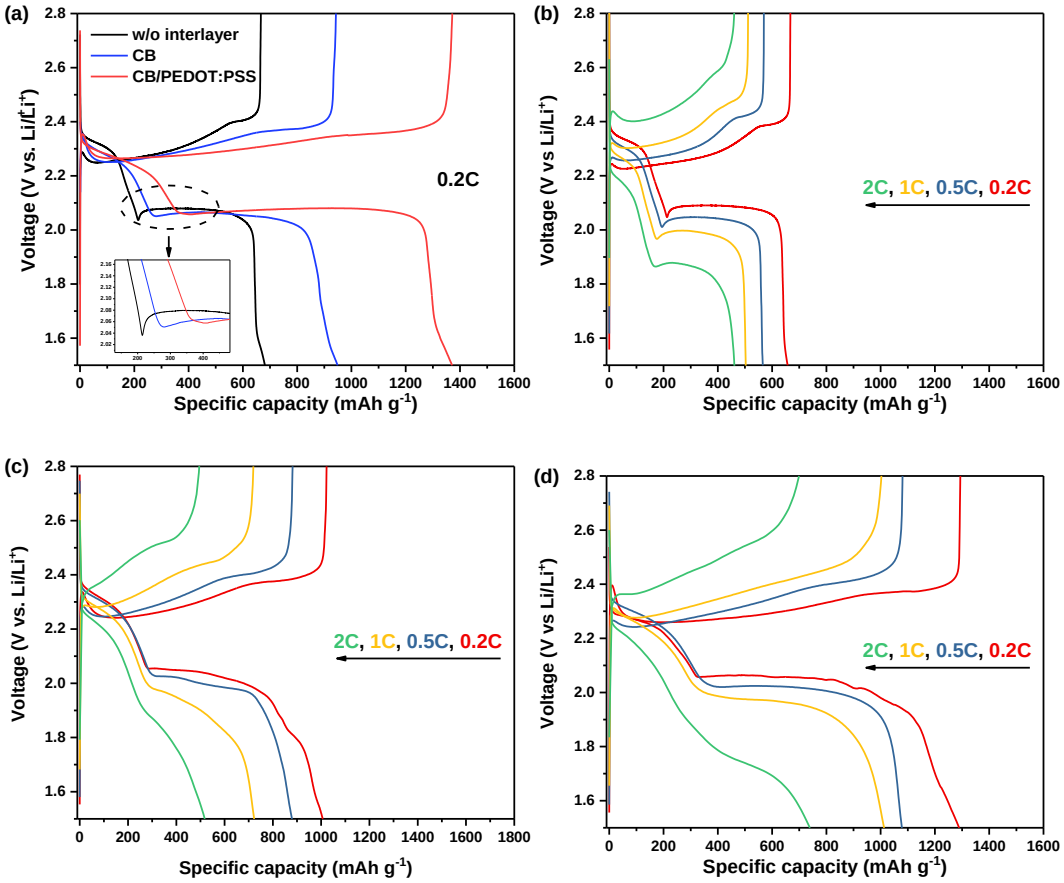

Fig. 2. Charge and discharge profiles (a) at 0.2 C the second cycle of cell without interlayer, with CB and CB/PEDOT:PSS interlayers. The insert shows the enlarged part where two discharge plateaus meet, (b) at different rates of cell without interlayer, (c) at different rates of cell with CB, (d) at different rates of cell with CB/PEDOT:PSS interlayers.

The cyclic voltammetry (CV) profiles of pristine cell and cell with CB/PEDOT:PSS interlayer help to clarify how this interlayer facilitates the redox kinetic, as shown in Fig. 3. The CV curves show two prominent cathodic peaks and one anodic peak, which are typical for Li-S batteries. The cathodic peaks are related to the lithiation process from S_8 to long-chain polysulfides (2.2~2.3V, Peak B) and the subsequent reduction to the insoluble short-chain polysulfides (1.9-2.0V, Peak C), while anodic peaks (2.3-2.5V, Peak A) are attributed to the reverse oxidation process [44, 45]. It is clear from Fig. 3 that cell with CB/PEDOT:PSS coating shows decreased voltage hysteresis, and the corresponding voltage differences between cathodic peaks and anodic peaks (ΔE_A and

ΔE_B) are significantly reduced in the CB/PEDOT:PSS cell (ΔE_{A2} = 0.500 V → ΔE_{A1} = 0.388 V and ΔE_{B2} = 0.222 V → ΔE_{B1} = 0.105 V). This can be explained by the effect of co-current collector provided by the CB/PEDOT:PSS coating, which leads to the improved electrochemical kinetics and decreased polarization. What's more, the higher values of specific peak current of CB/PEDOT:PSS cell also confirm that the CB/PEDOT:PSS coating helps to maximize the utilization of active material. This is due to the outstanding polysulfides-trapping ability of this coating, as well as the improved Li ion transport, which will be further proved by the subsequent results.

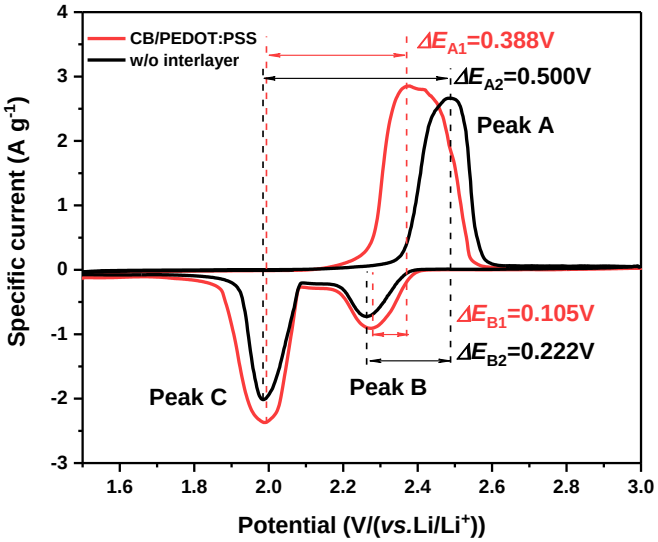

Fig. 3. Cyclic voltammetry profiles of pristine cell and cell with CB/PEDOT:PSS interlayer for the first cycle.

The cyclic performances measured at 0.2 C of three different cells are compared in Fig. 4a. Both cells with pure CB and CB/PEDOT:PSS interlayers exhibit much higher specific capacities than the cell without the interlayer. A significant high initial specific discharge capacity of 1315 mAh g^{-1} is delivered by the cell with CB/PEDOT:PSS interlayer, which is maintained at 956 mAh g^{-1} after 100 cycles with high capacity

retention of 72.7 % of the initial value. Correspondingly, the cell with CB interlayer shows capacities of 1019 mAh g^{-1} and 718 mAh g^{-1}, with capacity retention of 70.4 % under the same condition. In comparison, the pristine Li-S cell without the interlayer shows an initial capacity of 682 mAh g^{-1} and a cycled capacity of 321 mAh g^{-1} with a poor retention of 47.1 %. The cell with CB/PEDOT:PSS interlayer exhibits much superior electrochemical performance, which is also better than the cell with CB interlayer. This can be ascribed to the synergies from this dual-functional interlayer, including (i) the much better electron/ion transfer associated with the high electrical conductivity and porosity of CB/PEDOT:PSS interlayer, (ii) the heterogeneous atoms in PEDOT (thiophenic sulfur and ethylenedioxy R–O–O–R' group) which have strong interactions with soluble polysulfide species to entrap them [17], (iii) the $-SO_3^-$ functional group of the PSS provides the hopping channel for Li ion, and this mechanism facilitates the redox at high current density [27].

A further test on rate performance of different cells has provided additional evidence that the cell with CB/PEDOT:PSS interlayer performed better than the cell with pure CB interlayer under various rates. As seen in Fig. 4 (b), the cells were evaluated by increasing the C-rate from 0.2 C to 2 C, and then gradually back to 0.2 C. For the cell employing the CB/PEDOT:PSS interlayer, a specific capacity of 1293 mAh g^{-1}, 1080 mAh g^{-1}, 1002 mAh g^{-1} and 699 mAh g^{-1} was achieved at 0.2 C, 0.5 C, 1 C and 2 C, respectively, much higher than the one with CB interlayer (990, 879, 722 and 517 mAh g^{-1} at 0.2, 0.5, 1 and 2 C). When the rate returns to 0.2 C after 60 cycles, a high reversible capacity of 1127 mAh g^{-1} is recovered, corresponding to a capacity retention

of 84.6%. As the rate capability is related to the kinetic of the cell, these results indicate the CB/PEDOT:PSS interlayer is more efficient in accelerating the velocity of the redox reaction in the Li-S cell. This advantage is further demonstrated by the long-term cycling test at 1 C, as shown in Fig. 4c. After 260 cycles the cell with CB/PEDOT:PSS interlayer still delivers a capacity of 674 mAh g^{-1}, while the pristine cell only shows 370 mAh g^{-1}. Notably, the areal density of CB/PEDOT:PSS coating is only 0.604 mg cm^{-2} as low, bringing an outstanding specific capacity of 522 mAh g^{-1} at 1 C based on the total mass of electrode materials and interlayer. Therefore, it can be concluded that the PEDOT:PSS have prominent positive effect on conventional sulfur cathode. All cells showed high Coulombic efficiencies in the range of 95-100%.

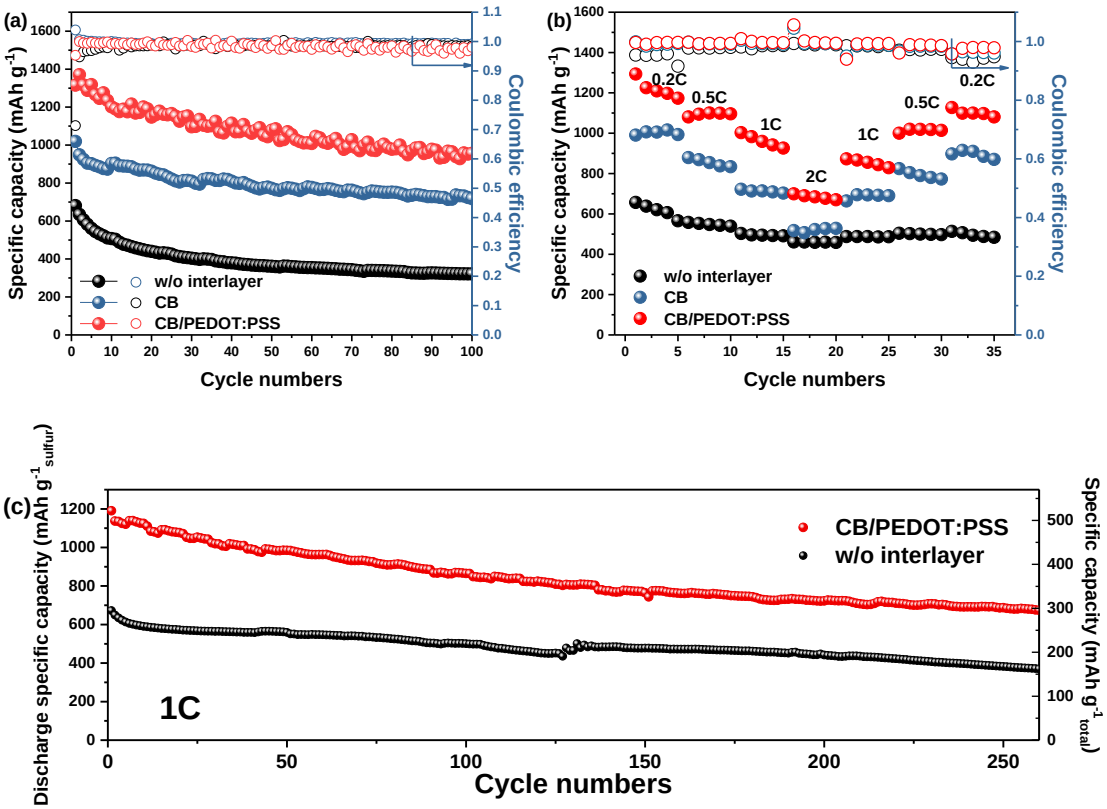

Fig. 4. (a) The cyclic discharging specific capacities and Coulombic efficiency of cell without interlayer, with CB or CB/PEDOT:PSS interlayer at 0.2 C current density. (b) The rate capacities of cells with CB or CB/PEDOT:PSS interlayer. (c) Long-term cycling of CB/PEDOT:PSS cell at 1 C.

To demonstrate the polysulfides-trapping ability, a special isolated cell was assembled and tested at 0.2 C, in which an additional separator was placed between cathode and CB/PEDOT:PSS coating so that the coating was electrically isolated from electrodes but saturated with electrolyte [44], as shown in Fig. S3. Compared with the CB/PEDOT:PSS cell, the isolated cell showed a degraded initial specific capacity of 1113 mAh g^{-1}, and ended with 609 mAh g^{-1} after 100 cycles. This drop of the capacity gives a further indication that the important role of the CB/PEDOT:PSS interlayer in sulfur utilization of the cell. It is also interesting to note that the Coulombic efficiency of the isolated cell continues to decline with cycles, and it drops to less than 0.9 after 100 cycles. The reason here is probably related to the dissolved polysulfides anchored by the CB/PEDOT:PSS coating during discharging cannot be further reduced or oxidized due to the isolation. Subsequently, a growing amount of active materials is accumulated and isolated in the CB/PEDOT:PSS layer, resulting in the fall of Coulombic efficiency. Cells with isolated interlayer and with 2 layers of separator show similar capacities for the initial 5 cycles, and both of them show lower capacity than the CB/PEDOT:PSS cell due to the absence of the “co-current collector” effect. As the cycle goes on, the 2-layer-separator cell degrades more rapidly than the CB/PEDOT:PSS one. This is ascribed to the polysulfide absorption effect of the isolated interlayer that reduces the shuttle effect. These differences in capacity and Coulombic efficiency demonstrate the polysulfides trapping-ability of the CB/PEDOT:PSS coating in an indirect approach.

To quantify how much the modified separator promotes Li ion transference, a series

of CV tests are conducted on cells with CB/PEDOT:PSS interlayer at different scanning rates (Fig. 5). All the cathodic and anodic peak currents are linear with the square root of scan rate (Fig. 5b, d), indicating that the reactions are diffusion-controlled [31]. The Randles−Sevcik equation was adopted to calculate the diffusion coefficients (D_{Li^+}) [23, 31],

$$I_{\mathrm{p}} = 2.69 \times 10^5 n^{1.5} A {D_{Li^+}}^{0.5} C \nu^{0.5} \quad (1)$$

Where I_{p} is the peak current, n is the electron transfer number during the reaction (n = 2 for Li-S batteries), A is the electrode surface area (cm^2, which is undetermined in this porous sulfur cathode), D_{Li^+} is the diffusion coefficient of Li cation ($cm^2\ s^{-1}$), C is the concentration of Li cation in electrolyte (mol mL^{-1}), and ν is the scan rate ($V\ s^{-1}$). The Li ion diffusion coefficients of pristine cell and cell with CB/PEDOT:PSS modified separator were calculated and summarized in Table 1. It can be seen that the diffusion coefficients of lithium ion in the CB/PEDOT:PSS covered cathode are significantly higher than those in the pristine Li-S cell. Coefficients have grown by 167.8%, 144.7% and 45.5% for peak A, B and C, respectively (Table 1). This suggested that the redox reactions, especially the anodic reaction $Li_2S/Li_2S_2 \rightarrow S_8$ and cathodic reaction $S_8 \rightarrow Li_2S_8$ are remarkably enhanced. This result demonstrates that the addition of the CB/PEDOT:PSS modified separator does not hinder the transport of Li cation, but in fact improves it. This prominent increase in Li ion diffusion coefficients is probably ascribed to the sulfonate groups in PSS that allow for accelerating the Li cation transport during cycling [46].

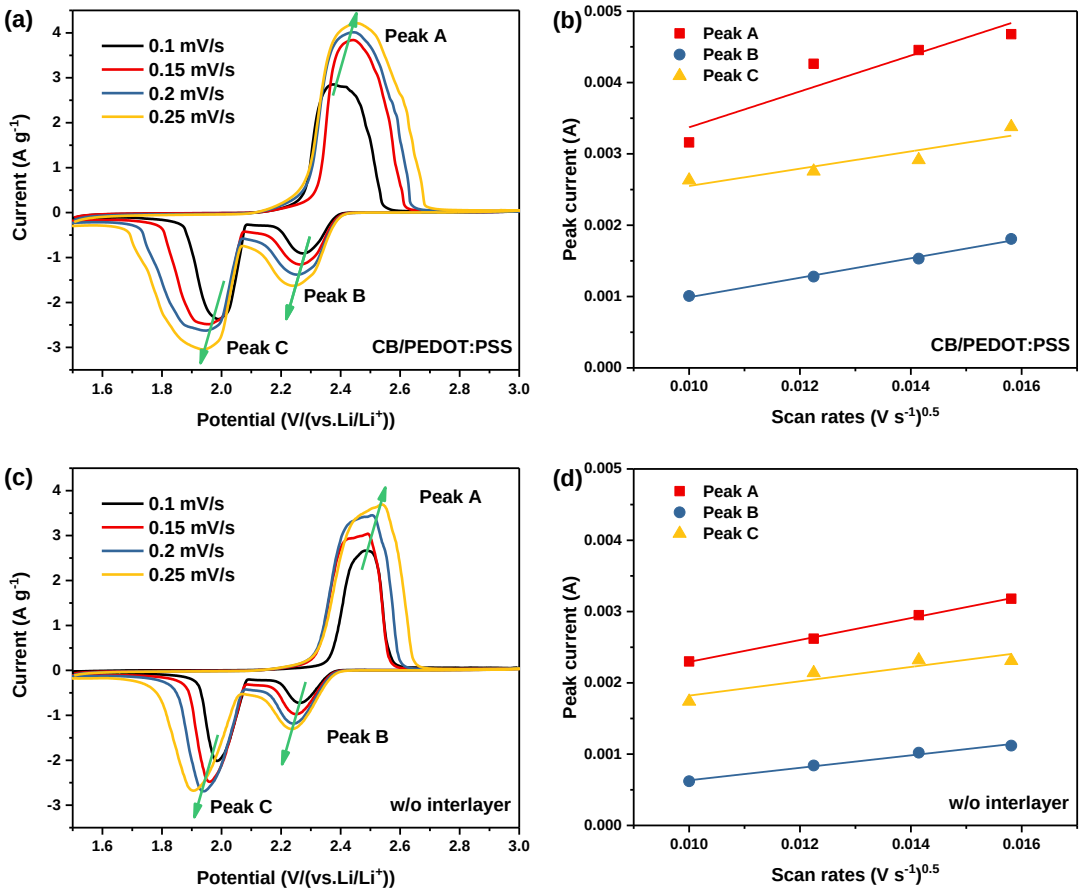

Fig. 5. CV curves recorded at different scan rates for Li–S batteries with (a) CB/PEDOT:PSS modified separator and (c) without interlayer. Linear fits of CV peak current dependences based on the scan rate of Li–S batteries with (b) CB/PEDOT:PSS modified separator and (d) without interlayer.

Table 1 The calculated Li ion diffusion coefficients of pristine cell and cell with CB/PEDOT:PSS modified separator.

Diffusion coefficient D_{Li^+}	Peak A/cm^4 s^{-1}	Peak B/ cm^4 s^{-1}	Peak C/ cm^4 s^{-1}
w/o interlayer	$4.11 \times 10^{-8} \times A^{-2}$	$1.32 \times 10^{-8} \times A^{-2}$	$1.75 \times 10^{-8} \times A^{-2}$
CB/PEDOT:PSS	$11.01 \times 10^{-8} \times A^{-2}$	$3.24 \times 10^{-8} \times A^{-2}$	$2.47 \times 10^{-8} \times A^{-2}$
Ratio of D_{Li^+} between two cells	267.8%	244.7%	145.5%

To understand the mechanism of how the interlayer traps the polysulfide intermediates, the XPS measurement was conducted on both pristine and cycled CB/PEDOT:PSS interlayer, as shown in Fig. 6. The wide survey scans before cyclic test and after 50 cycles both present seven main peaks located at 168, 231, 285, 400,

532 and 689 eV which correspond to S 2*p*, S 2*s*, C 1*s*, N 1*s*, O 1*s* and F 1*s*, respectively (Fig. 6a). It is noted that in the cycled spectrum the S 2*p* and S 2*s* peaks are more intense than those in the pristine one, indicating the deposition of active materials on the interlayers. There is one extra N 1*s* peak at 400 eV in the cycled spectrum plus with stronger intensities of the O 1*s* and F 1*s* peaks, probably rising from the $LiNO_3$ and LiTFSI salts in the remnant electrolyte.

The deconvoluted S 2*p* spectra (Fig. 6b) obtained before cycles present two split broad peaks at around 169 and 165 eV, corresponding to the S 2*p* bands of PSS and PEDOT moieties, respectively [47-49]. After 50 cycles, the spectrum shows much stronger bands in the range of 168-172 eV, which can be assigned to the O=S=O bonds from the remnant LiTFSI salts. The thiosulfate -S-S*O_3 band at 167.4 eV may be originated from the oxidation of the polysulfides by $LiNO_3$ [50]. The Li-S and S-S bands in the range of 162-166 eV are clearly identified [50]. For the Li *1s* spectra (Fig. 6d and e), a prominent peak emerges after cycling. The deconvoluted result suggests a Li-O bond (55.4 eV) [51] ,which indicates the chemical absorption between the lithium in polysulfide and the oxygen in PEDOT:PSS. An additional Li-N peak (55.6 eV) [52] is from the residual LiTFSI in the electrolyte.

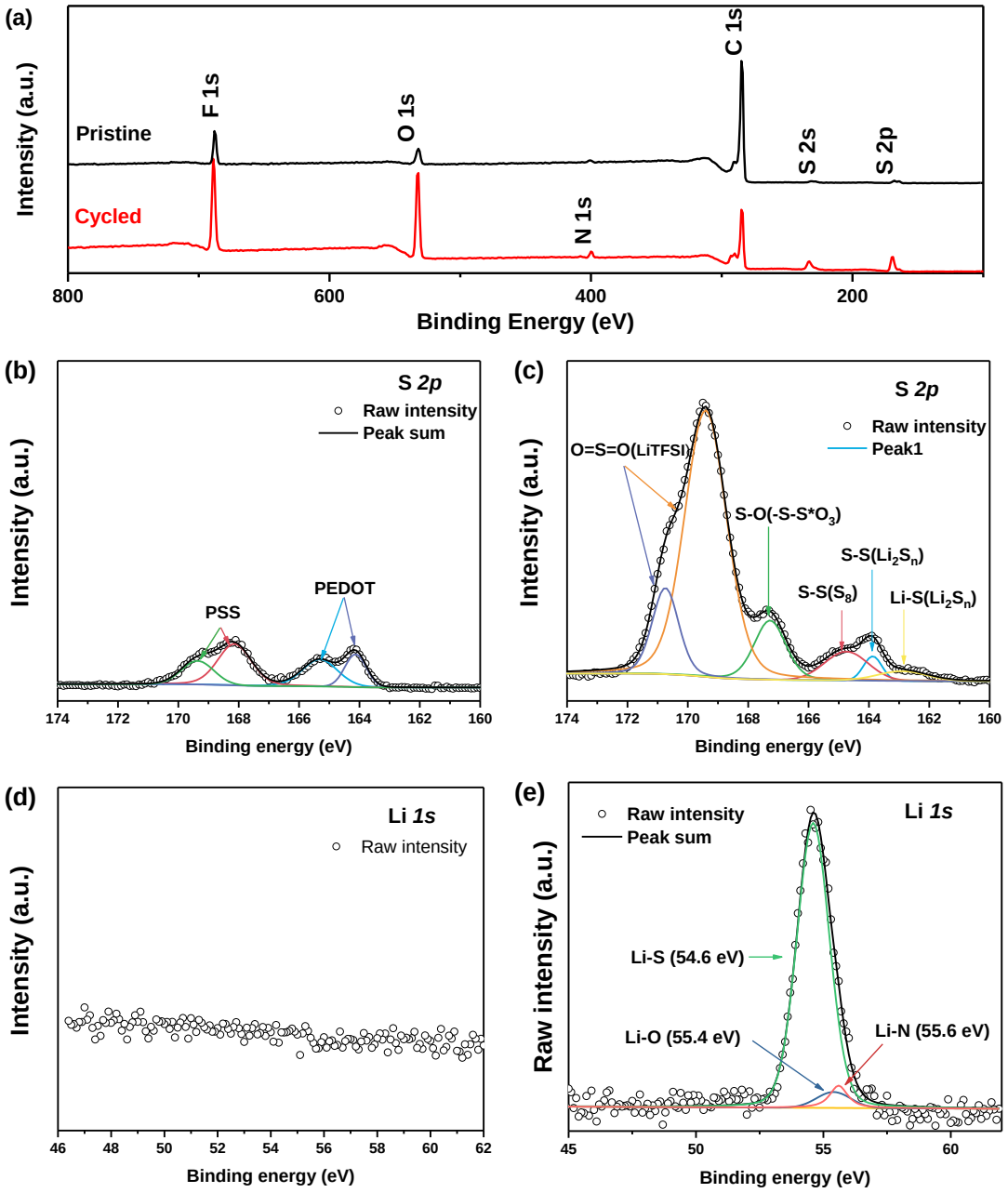

Fig. 6. (a)The wide survey spectra of CB/PEDOT interlayer before and after 50 cycles at 0.5 C. The deconvoluted S *2p* and Li *1s* XPS spectrum of (b)(d) Pristine CB/PEDOT:PSS interlayer and (c)(e) CB/PEDOT:PSS interlayer after 50 cycles at 0.5 C.

The Nyquist plots of different cells before and after 10 cycles at 0.2 C are shown in Fig. 7. In the Nyquist plots, the diameter of the depressed semicircle in the high-to-medium frequency region corresponds to charge-transfer resistance (R_{ct}) from the electrochemical reaction between the electrode and electrolyte [53], while the sloping line in the low-frequency region is assigned to the semi-infinite Warburg impedance

(Wo), which reflects the diffusion process of the polysulfides within the cathode [54, 55]. In the corresponding circuits, the R_e represents the resistance of the electrolyte. The sum of R_e, R_{ct} and R_{st} is calculated as the total resistance of the cell (R_{total}). According to the fitted results (Table 2), the most prominent difference between these two cells is the shrinkage in R_{ct} values after adding the interlayers. This amelioration should be ascribed to the highly conductive few-layer graphene foam that acts as the co-current collector, which greatly facilitates the redox of dissolved polysulfides. The low R_{ct} value of cell with CB/PEDOT:PSS interlayer indicates the highest efficiency of CB/PEDOT:PSS interlayer in reutilizing polysulfides. It is noticeable that an additional arc at medium frequency appears at the EIS of the cycled cell without interlayer, indicating that excessive lithium sulfides deposits on the surface after cycles. Meanwhile, cells with interlayer exhibit only one arc after cycles, and the CB/PEDOT:PSS cell shows the lowest R_{total} value. The low R_{total} value of the cell with CB/PEDOT:PSS interlayer is another evidence of the remarkable effect on reducing the internal resistance.

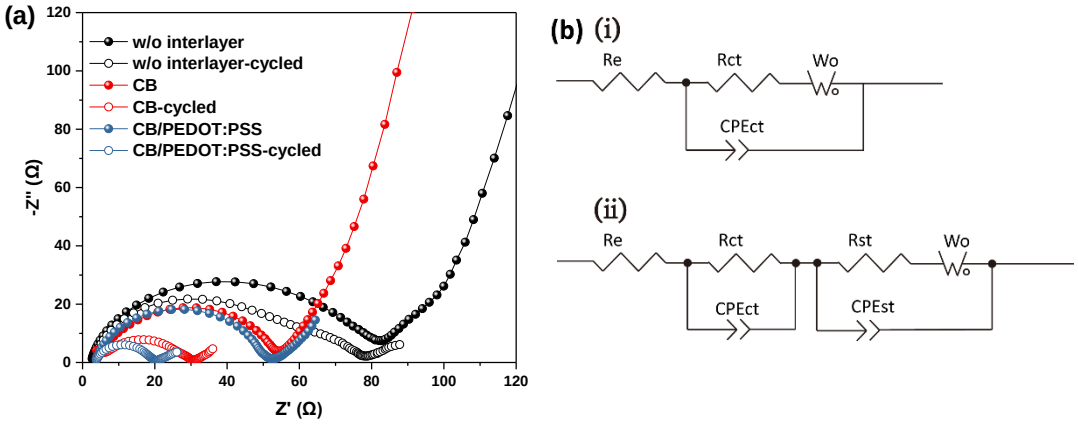

Fig. 7. (a) Electrochemical impedance spectra of pristine Li-S cell and cells with CB and

CB/PEDOT:PSS interlayers before and after 10 cycles at 0.2 C. (b) The corresponding equivalent circuits of all the cells (i) except the cycled cell without interlayer (ii)

Table 2 Fitted values of the impedance spectra in Fig. 7

		R_e(Ω)	R_{ct} (Ω)	R_{st} (Ω)	R_{total} (Ω)
Cell without interlayer	pristine	1.99	79.3	/	81.3
	cycled	3.24	46.3	29.4	78.9
Cell with CB interlayer	pristine	4.10	50.5	/	54.6
	cycled	4.94	25.2	/	30.1
Cell with CB/PEDOT:PSS interlayer	pristine	3.57	47.8	/	51.4
	cycled	3.41	16.7	/	20.1

Conclusion

The CB/PEDOT:PSS modified separator was proposed and fabricated using a facile one-step physical approach which favours practical production, due to its low-cost and scalable process. The bi-functional modified separator not only serves as a secondary current collector, but also an effective polysulfides-trapper, owing to both physical and chemical absorption provided by super-P and PEDOT:PSS. In addition, this modification coating promotes chemical kinetic by enhancing Li ion diffusion. As a result, the primitive S-C electrode with sulfur loading of 1.6 mg cm^{-1} exhibits a high initial capacity of 1315 mAh g^{-1} at 0.2 C after the application of modified separator, maintaining a retention of 956 mAh g^{-1} after 100 cycles. Even after 260 cycles at 1 C, this modified cell still holds a considerable capacity of 674 mAh g^{-1}. More surprisingly, the areal density of CB/PEDOT:PSS coating is only 0.604 mg cm^{-2} as low, bringing an outstanding specific electrode capacity of 522 mAh g^{-1} based on the total mass of electrode materials and the interlayer, which further proves its potential application in practical high performance Li-S batteries.

Acknowledgement

This work was supported by the National Natural Science Foundation of China (NSFC Grants 21750110441), Suzhou Industrial Park Initiative Platform Development for Suzhou Municipal Key Lab for New Energy Technology (RR0140), and Key Program Special Fund in XJTLU (KSF-A-04 and KSF-E-28).

References

[1] X. Ji, L.F. Nazar, *J. Mater. Chem.* **2010**, *20*, 9821-9826.

[2] H. Zhao, N. Deng, J. Yan, W. Kang, J. Ju, Y. Ruan, X. Wang, X. Zhuang, Q. Li, B. Cheng, *Chem. Eng. J.* **2018**, *347*, 343-365.

[3] J. Scheers, S. Fantini, P. Johansson, *J. Power Sources* **2014**, *255*, 204-218.

[4] S.-K. Lee, Y.J. Lee, Y.-K. Sun, *J. Power Sources* **2016**, *323*, 174-188.

[5] J. Zhang, H. Huang, J. Bae, S.-H. Chung, W. Zhang, A. Manthiram, G. Yu, *Small Methods* **2018**, *2*, 1700279-1700310.

[6] X. Ji, K.T. Lee, L.F. Nazar, *Nat. Mater.* **2009**, *8*, 500-506.

[7] O.S.G.P. Soares, R.P. Rocha, A.G. Gonçalves, J.L. Figueiredo, J.J.M. Órfão, M.F.R. Pereira, *Carbon* **2015**, *91*, 114-121.

[8] S.C. Han, M.S. Song, H. Lee, H.S. Kim, H.J. Ahn, J.Y. Lee, *J. Electrochem. Soc.* **2003**, *150*, A889-A893.

[9] R. Fang, G. Li, S. Zhao, L. Yin, K. Du, P. Hou, S. Wang, H.-M. Cheng, C. Liu, F. Li, *Nano Energy* **2017**, *42*, 205-214.

[10] D. Su, M. Cortie, G. Wang, *Adv. Energy Mater.* **2016**, 1602014-1602025.

[11] Y. Hwa, H.K. Seo, J.M. Yuk, E.J. Cairns, *Nano Lett.* **2017**, *17*, 7086-7094.

[12] F. Wu, J. Li, Y. Su, J. Wang, W. Yang, N. Li, L. Chen, S. Chen, R. Chen, L. Bao, *Nano Lett.* **2016**, *16*, 5488-5494.

[13] G. Ma, Z. Wen, J. Jin, Y. Lu, K. Rui, X. Wu, M. Wu, J. Zhang, *J. Power Sources* **2014**, *254*, 353-359.

[14] N. Jayaprakash, J. Shen, S.S. Moganty, A. Corona, L.A. Archer, *Angew. Chem. Int. Ed.* **2011**, *50*, 5904-5908.

[15] X. Wang, C. Yang, X. Xiong, G. Chen, M. Huang, J.-H. Wang, Y. Liu, M. Liu, K. Huang, *Energy Storage Mater.* **2019**, *16*, 344-353.

[16] Z. Cui, C. Zu, W. Zhou, A. Manthiram, J.B. Goodenough, *Adv. Mater.* **2016**, *28*, 6926-6931.

[17] W. Li, Q. Zhang, G. Zheng, Z.W. Seh, H. Yao, Y. Cui, *Nano Lett.* **2013**, *13*, 5534-5540.

[18] W. Zhou, Y. Yu, H. Chen, F.J. DiSalvo, H.D. Abruna, *J. Am. Chem. Soc.* **2013**, *135*, 16736-16743.

[19] L. Xiao, Y. Cao, J. Xiao, B. Schwenzer, M.H. Engelhard, L.V. Saraf, Z. Nie, G.J. Exarhos, J. Liu, *Adv. Mater.* **2012**, *24*, 1176-1181.

[20] J.-Q. Huang, Q. Zhang, F. Wei, *Energy Storage Mater.* **2015**, *1*, 127-145.

[21] Q. Zhao, Q. Zhu, Y. An, R. Chen, N. Sun, F. Wu, B. Xu, *Appl. Surf. Sci.* **2018**, *440*, 770-777.

[22] T. Zhao, Y. Ye, X. Peng, G. Divitini, H.-K. Kim, C.-Y. Lao, P.R. Coxon, K. Xi, Y. Liu, C. Ducati, R. Chen, R.V. Kumar, *Adv. Funct. Mater.* **2016**, *26*, 8418-8426.

[23] K. Wu, Y. Hu, Z. Shen, R. Chen, X. He, Z. Cheng, P. Pan, *J. Mater. Chem. A* **2018**, *6*, 2693-2699.

[24] Y.S. Su, A. Manthiram, *Chem. Commun. (Camb.)* **2012**, *48*, 8817-8819.

[25] Q. Wang, Z. Wen, J. Yang, J. Jin, X. Huang, X. Wu, J. Han, *J. Power Sources* **2016**, *306*, 347-353.

[26] J. Balach, T. Jaumann, M. Klose, S. Oswald, J. Eckert, L. Giebeler, *Adv. Funct. Mater.* **2015**, *25*, 5285-5291.

[27] Z. Hao, L. Yuan, Z. Li, J. Liu, J. Xiang, C. Wu, R. Zeng, Y. Huang, *Electrochim. Acta* **2016**, *200*, 197-203.
[28] H. Yao, K. Yan, W. Li, G. Zheng, D. Kong, Z.W. Seh, V.K. Narasimhan, Z. Liang, Y. Cui, *Energy Environ. Sci.* **2014**, *7*, 3381-3390.
[29] G. Ma, Z. Wen, J. Jin, M. Wu, X. Wu, J. Zhang, *J. Power Sources* **2014**, *267*, 542-546.
[30] Z. Xiao, Z. Yang, L. Wang, H. Nie, M. Zhong, Q. Lai, X. Xu, L. Zhang, S. Huang, *Adv. Mater.* **2015**, *27*, 2891-2898.
[31] Z. Liu, B. Liu, P. Guo, X. Shang, M. Lv, D. Liu, D. He, *Electrochim. Acta* **2018**, *269*, 180-187.
[32] H. Shao, W. Wang, H. Zhang, A. Wang, X. Chen, Y. Huang, *J. Power Sources* **2018**, *378*, 537-545.
[33] X. Zhao, J.-K. Kim, H.-J. Ahn, K.-K. Cho, J.-H. Ahn, *Electrochim. Acta* **2013**, *109*, 145-152.
[34] F. Wu, J. Chen, L. Li, T. Zhao, R. Chen, *J. Phys. Chem. C* **2011**, *115*, 24411-24417.
[35] J. Wang, S. Cheng, W.F. Li, L.J. Jia, Q.B. Xiao, Y. Hou, Z.Z. Zheng, H.F. Li, S. Zhang, L.S. Zhou, M.N. Liu, H.Z. Lin, Y.G. Zhang, *Nano Energy* **2017**, *40*, 390-398.
[36] P. Xiao, F. Bu, G. Yang, Y. Zhang, Y. Xu, *Adv. Mater.* **2017**, *29*, 1703324-1703328.
[37] H. Chen, W. Dong, J. Ge, C. Wang, X. Wu, W. Lu, L. Chen, *Sci. Rep.* **2013**, *3*, 1910-1915.
[38] G. Ma, Z. Wen, Q. Wang, C. Shen, P. Peng, J. Jin, X. Wu, *J. Power Sources* **2015**, *273*, 511-516.
[39] L. Yin, H. Dou, A. Wang, G. Xu, P. Nie, Z. Chang, X. Zhang, *New J. Chem.* **2018**, *42*, 1431-1436.
[40] A.X. Wang, G.Y. Xu, B. Ding, Z. Chang, Y. Wang, H. Dou, X.G. Zhang, *ChemElectroChem* **2017**, *4*, 362-368.
[41] J. Zhu, Y. Ge, D. Kim, Y. Lu, C. Chen, M. Jiang, X. Zhang, *Nano Energy* **2016**, *20*, 176-184.
[42] K. Zhang, Q. Li, L. Zhang, J. Fang, J. Li, F. Qin, Z. Zhang, Y. Lai, *Mater. Lett.* **2014**, *121*, 198-201.
[43] S. Park, R.S. Ruoff, *Nat. Nanotechnol.* **2009**, *4*, 217-224.
[44] R. Yi, C. Liu, Y. Zhao, L.J. Hardwick, Y. Li, X. Geng, Q. Zhang, L. Yang, C. Zhao, *Electrochim. Acta* **2019**, *299*, 479-488.
[45] L. Tan, X. Li, Z. Wang, H. Guo, J. Wang, *ACS Appl. Mater. Interfaces* **2018**, *10*, 3707-3713.
[46] P. Han, S.-H. Chung, A. Manthiram, *Energy Storage Mater.* **2018**, *17*, 317-324.
[47] H. Yan, H. Okuzaki, *Synth. Met.* **2009**, *159*, 2225-2228.
[48] X. Wang, Z. Zhang, Y. Qu, Y. Lai, J. Li, *J. Power Sources* **2014**, *256*, 361-368.
[49] J. Hwang, F. Amy, A. Kahn, *Org. Electron.* **2006**, *7*, 387-396.
[50] P. Zeng, L. Huang, X. Zhang, R. Zhang, L. Wu, Y. Chen, *Chem. Eng. J.* **2018**, *349*, 327-337.
[51] Y. Chen, S. Lu, J. Zhou, X. Wu, W. Qin, O. Ogoke, G. Wu, *J. Mater. Chem. A* **2017**, *5*, 102-112.
[52] Z.W. Seh, H. Wang, P.-C. Hsu, Q. Zhang, W. Li, G. Zheng, H. Yao, Y. Cui, *Energy Environ. Sci.* **2014**, *7*, 672-676.
[53] J.Q. Huang, Z. Wang, Z.L. Xu, W.G. Chong, X. Qin, X. Wang, J.K. Kim, *ACS Appl. Mater. Interfaces* **2016**, *8*, 28663-28670.
[54] M. Wang, H. Zhang, W. Zhou, X. Yang, X. Li, H. Zhang, *J. Mater. Chem. A* **2016**, *4*, 1653-1662.
[55] J. Xu, D. Su, W. Zhang, W. Bao, G. Wang, *J. Mater. Chem. A* **2016**, *4*, 17381-17393.